Digest Journal of Nanomaterials and Biostructures

Dig. J. Nanomater. Bios. **2026**; 21(4): 54355
https://doi.org/10.31083/DJNB54355

Original Research

Green Synthesis of *Smilax china*-Mediated CuO–ZnO Bimetallic Nanoparticles and ROS-Mediated Anti-Cancer Activity in Saos-2 Osteosarcoma Cells

Essa M. Sabi[1,*], Ahmed H. Mujamammi[1], Khalid M. Sumaily[1], Khalil I. Zarea[2], Ziyad M. Althafar[3]

[1]Clinical Biochemistry Unit, Department of Pathology, College of Medicine, King Saud University, 11461 Riyadh, Saudi Arabia
[2]Department of Physical Sciences, Chemistry Division, College of Science, Jazan University, 45142 Jazan, Saudi Arabia
[3]Department of Medical Laboratories Sciences, College of Applied Medical Sciences in Alquwayiyah, Shaqra University, 11961 Riyadh, Saudi Arabia
*Correspondence: esabi@ksu.edu.sa (Essa M. Sabi)

Academic Editor: Karol Kyzioł
Submitted: 30 May 2026 Revised: 11 July 2026 Accepted: 16 July 2026 Published: 11 November 2026

Abstract

Background: Osteosarcoma (OS) is one of the most aggressive primary bone cancers that commonly affects adolescents and children. Regardless of advances in treatment, the effectiveness of current therapies is often limited by drug resistance and severe side effects, which makes the development of safer and more potent therapeutic strategies an important research priority. **Methods:** CuO–ZnO nanoparticles were synthesized in a green way using *Smilax china* rhizome extract and evaluated for anti-cancer activity against osteosarcoma (Saos-2) cells. Nanoparticle structure and morphology were probed by ultraviolet (UV)–visible spectroscopy, Fourier transform infrared spectroscopy (FTIR), X-ray diffraction (XRD), scanning electron microscopy (SEM), and energy-dispersive X-ray spectroscopy (EDAX). Cytotoxicity concentrations were determined using the 3-(4,5-dimethylthiazol-2-yl)-2,5-diphenyltetrazolium bromide (MTT) test. Trypan blue staining was used to examine cell viability. Oxidative stress markers—reactive oxygen species (ROS), lipid peroxidation (LPO), and reduced glutathione (GSH)—were analyzed to understand the origin of anti-cancer activity. Flow cytometry was used to analyze the cell cycle, and fluorescence measurements with 4′,6-diamidino-2-phenylindole (DAPI) and 2′,7′-dichlorodihydrofluorescein diacetate were employed to characterize apoptotic alterations and intracellular ROS production. **Results:** Physicochemical characterization verified the synthesis of quasi-spherical crystalline CuO–ZnO nanoparticles stabilized by phytoconstituents. The nanoparticles showed notable dose-dependent cytotoxicity in Saos-2 cells. ROS analysis and DAPI staining revealed the presence of apoptotic cells. Elevated LPO levels, along with a marked reduction in intracellular GSH, indicated oxidative stress–mediated cellular damage. The nanoparticles (NPs) exposure leads to increase the free radical liberation in Saos-2 cells, thus increasing caspase activity. Flow cytometry analysis revealed cell cycle arrest at the G0/G1 phase and S phase, suggesting the inhibition of cell proliferation. Furthermore, the scratch assay demonstrated a significant suppression of cell migration compared with control cells. **Conclusions:** CuO–ZnO nanoparticles prepared using *Smilax china* extract exerted significant anti-cancer activity against osteosarcoma cells through ROS-mediated oxidative stress and apoptotic pathways and were concluded to hold promise for osteosarcoma treatment.

Keywords: *Smilax china*; osteosarcoma; metal oxides; bimetallic nanoparticles; ROS-mediated apoptosis; oxidative stress

1. Introduction

Osteosarcoma (OS) is the most common primary malignant bone tumor, primarily affecting children and young people. The prognosis of patients are greatly impacted by their high tendency and quick expansion. The overall survival rate for individuals with osteosarcoma has only slightly increased in recent years, despite multimodal treatment options such as chemotherapy, radiotherapy, and surgery. The development of multidrug resistance (MDR) in tumor cells, significant systemic toxicity and a lack of selective action against cancer cells that results in damage to healthy tissues are some of the primary issues with traditional chemotherapeutic drugs that contribute to this impasse. This stagnation is largely attributed to several critical limitations associated with conventional chemotherapeutic drugs, such as severe systemic toxicity, the development of MDR in tumor cells, and a lack of selective action against cancer cells, leading to collateral damage to healthy tissues. These limitations necessitate alternative therapeutic approaches that enhance both safety and effectiveness [1,2]. Nanotechnology-based cancer therapies enabled enhanced cellular uptake, targeted cytotoxicity, and modification of cancer-specific molecular pathways, thereby overcoming these barriers. Specifically, metal-based nanoparticles have shown strong anti-cancer potential through mechanisms including DNA damage, mitochondrial dysfunction, induction of apoptosis, and reactive oxygen species (ROS) generation [3]. In the field of nanomedicine, metal oxide nanoparticles (MONPs) are gaining significant attention due to their unique physicochemical properties and biological potential. Their enormous surface area and nanoscale

Copyright: © 2026 The Author(s). Published by IMR Press.
This is an open access article under the CC BY 4.0 license.

Publisher's Note: IMR Press stays neutral with regard to jurisdictional claims in published maps and institutional affiliations.

size enable them to interact effectively with biological systems and medications. For the delivery of medication and cancer treatment, MONPs like ZnO, CuO and iron oxide are being extensively researched. These nanoparticles (NPs) have the capacity to generate reactive oxygen species, which causes oxidative stress and cell death. MONPs are attractive options for targeted anti-cancer applications due to their biocompatibility and potential for surface functionalization [4,5,6]. Bimetallic NPs have better biological performance than monometallic systems because of the synergistic interactions between two different metals, which lead to increased stability, redox activity and anti-cancer efficacy [7].

Copper and Zinc nanoparticles are bimetallic systems that have attracted considerable attention for biomedical applications. Zinc NPs regulate the DNA synthesis, cell cycle progression, and signaling linked to apoptosis, whereas copper NPs are known to cause oxidative stress and trigger intrinsic apoptosis pathways in cancer cells. It has been observed that combining copper and Zinc in a single nanostructure increases anti-cancer activity while preserving regulated cytotoxicity against healthy cells [5,8].

An essential component that determines the biological behavior of NPs is the fabrication process and there is a lot of interest in green synthesis as a sustainable and biocompatible technique that makes use of extracts from medicinal plants. Phytochemicals such as flavonoids, phenolic compounds, saponins, and alkaloids provide natural surface functionalization without the need for hazardous chemical reagents [9,10]. This bioactive substance enhances the stability, cellular absorption, and therapeutic action of nanoparticles by acting as a stabilizing and reducing agent.

Smilax china L. is widely used in traditional medicine and is rich in bioactive compounds, including phenolic constituents, steroidal saponins, and flavonoids. Its antioxidant, anti-inflammatory, anti-bacterial, and anti-cancer efficacy have been documented in earlier research, indicating its oxidative stress regulation and pathways linked to apoptosis [11,12]. Because of its rich phytochemical profile, *Smilax china* represents a promising natural source for the green synthesis of biologically active nanoparticles with enhanced anti-cancer potential. The human osteosarcoma Saos-2 cells exhibit characteristics of aggressive osteosarcoma, including a high proliferative capacity, resistance to apoptosis, and active osteogenic signaling. Hence, this cell line is widely used as an *in vitro* model to study the pathophysiology of bone cancer and to evaluate potential anti-cancer therapies [13].

Even though nanoparticle-based technologies were increasingly being explored for anti-cancer therapy, effective and safer therapies for osteosarcoma are still limited due to drug resistance and the toxicity associated with conventional chemotherapy. Metal oxide nanoparticles, such as CuO and ZnO, have shown promising anti-cancer potential; most studies have focused mainly on individual (monometallic) nanoparticles [8,14,15]. In addition, the medicinal plant *Smilax china*, which has numerous bioactive phytochemicals, has not been widely investigated for the green synthesis of bimetallic nanoparticles and their activity against osteosarcoma cells [11,12]. Hence, the aim of this study is to provide insights into the cytotoxic and mechanistic actions of *Smilax china*-mediated bimetallic CuO–ZnO nanoparticles, contributing to the development of potential bone cancer nano-therapies.

2. Methods

2.1 Preparation of Smilax china Extract

The fresh rhizome of *S. china* L. was carefully cleaned and ground into a fine powder. 10 g of the rhizome powder and 100 mL of distilled water were mixed and heated to 60 °C for 30 min while being continuously stirred. After filtering through Whatman No. 1 filter paper, the extract was stored at 4 °C for further use in the fabrication of NPs.

2.2 Fabrication of Bimetallic CuO–ZnO NPs

The *S. china* was used as a reducing and stabilizing agent in a green synthesis process. Zinc acetate dihydrates and Copper (II) sulfate pentahydrate salts were used to prepare an equal molar (0.01 M) solution in a 1:1 ratio and magnetically agitated. 10 mL of *S. china* extract was dropwise added to 90 mL of the metal solution at room temperature. After that, the mixture was kept at 60 ºC for two hours; the reaction mixture was cooled and centrifuged for twenty min at 12,000 rpm. The pellet was washed with deionized water, dried at 60 ºC, and kept in air-tight containers. The dried nanoparticles were accurately weighed using an analytical balance and subsequently dispersed in sterile distilled water to prepare a stock suspension of known concentration (mg/mL), which was further diluted to the required experimental concentrations.

2.3 Characterization of Synthesized Bimetallic (CuO–ZnO) Nanoparticles

The development of CuO–ZnO NPs was verified by using UV-visible spectroscopy, with the absorption spectra recorded in the 200–800 nm range. By identifying the functional groups on the NPs using Fourier transform infrared (FTIR) spectroscopy, which is examined between 400–4000 cm^{-1}. The size distribution profile was ascertained using the particle size analyzer (PSA), guaranteeing an accurate assessment of their physicochemical properties. Additionally, the successful integration of CuO and ZnO without impurities was confirmed by elemental analysis, and scanning electron microscopy (SEM) and energy-dispersive X-ray spectroscopy (EDAX) analysis were used to investigate the morphological characteristics of the nanoparticles. The crystallite quality of CuO–ZnO bimetallic NPs was analyzed by employing Rigaku Miniflex 600 X-ray diffractometer (Tokyo, Japan) with a high-power Cu K source operating at 40 kV/15 mA.

2.4 Cell Culture

The Saos-2 human Osteosarcoma cell line was obtained from the American Type Culture Collection (ATCC) (USA). We have tested for Mycoplasma using the PCR Mycoplasma Detection Set (Cat. No. 6601, TaKaRa, Kusatsu, Japan) and found it negative. The cell line has undergone STR identification. The cells were kept at 37 ºC in a humidified 5% CO_2 incubator in Dulbecco's modified Eagle medium (DMEM) supplemented with 10% fetal bovine serum (FBS), 100 U/mL penicillin, and streptomycin. Every two to three days, cells were subculture to maintain exponential growth.

2.5 MTT Assay

The anti-proliferative effect of *S. china*-derived CuO–ZnO nanoparticles and *S.China* ectracts on Saos-2 osteosarcoma cells was evaluated using an 3-(4,5-dimethylthiazol-2-yl)-2,5-diphenyltetrazolium bromide (MTT) assay [16]. Briefly, 1×10^5 cells were plated into 96-well culture plates and placed in the incubator overnight for cell attachment. The next day, the plates were replaced with fresh medium containing different concentrations of nanoparticle formulation (0.2 to 200 µg/mL) and extract (100–800 µg/mL) in seperate plates. The plates were returned to the incubator for another 24 h. At the end of the treatment, the MTT assay was performed on the plates. Briefly, MTT dye was prepared at a 5 mg/mL concentration and 100 µL of dye was added to each well. The plates were then placed in the incubator protected from light for 4 h for the formation of formazan crystals by metabolically active cells. The formazan crystals were then dissolved in Dimethyl Sulfoxide (DMSO) (100 µL), and the resulting purple colour was measured using a spectrophotometer at 570 nm. The percentage of growth inhibition was subsequently calculated using the following equation.

$$\% \text{ inhibition} = [1 - \{(Abs_{T490} - Abs_{T630}) - (Abs_{C490} - Abs_{C630})\} \times 100].$$

2.6 Trypan Blue Exclusion Assay

According to Crowley et al. [17], the trypan blue exclusion (TBE) assay was used to analyze the Saos-2 cell viability. Following standard culture conditions, cells were seeded into 96-well plates and allowed to adhere. After a 24-h stabilization period, cultures were exposed to *S. China*–CuO–ZnO nanoparticles at concentrations of 25, 50 and 75 µg/mL. Following treatment, both control and exposed cells were washed with Phosphate Buffer Solution, and cells were detached by using trypsin and re-suspended in fresh DMEM. A 0.4% trypan blue (TB) solution was then applied to stain non-viable cells, and cell counts were obtained using a hemocytometer to distinguish viable (unstained) from non-viable (stained) populations.

2.7 Morphometric Analysis

Morphometric assessment of control and treated Saos-2 cells was conducted following a slightly modified procedure adapted from Moongkarndi et al. [18]. Briefly, 5.25×10^5 cells were scattered and cultured for 24 h under standard conditions, after which they were exposed to *S. china*–CuO–ZnO nanoparticles at concentrations of 25, 50 and 75 µg/mL for an additional 24 h. Following treatment, the culture medium was discarded, and the cells were washed gently with PBS. Cellular morphology and structural alterations were then examined using a phase-contrast microscope.

2.8 DAPI Fluorescence Staining

Initially, 1×10^5 cells were seeded into a 24-well plate, and they were exposed to different concentrations (25, 50, and 75 µg/mL) of synthesized NPs. After exposure, the test and control groups were fixed with cooled methanol for 10 min and washed with cold PBS. Following 4% formaldehyde permeabilization, cells were stained with 4′,6-diamidino-2-phenylindole (DAPI) (0.5 µg/mL). A fluorescence microscope (Nikon, Tokyo, Japan) was used to take a nuclear fluorescence picture [19].

2.9 Determination of ROS

The 2′,7′-dichlorodihydrofluorescein Diacetate (DCFH-DA) fluorescent assay was used to analyze the intracellular ROS production [20]. Synthesized NPs doses ranging from 25 to 75 µg/mL were applied to Saos-2 cells grown in 24-well plates for 24 h. Following treatment, the cells were treated with 10 µM DCFH-DA for 30 min at 37 ºC after being rinsed with PBS. To record ROS accumulation, fluorescence images were captured using a fluorescence microscope after the dye was removed by washing.

2.10 Reduced Glutathione (GSH) Assay

Reduced glutathione was estimated with minor adjustments to the methodology of Goh et al. [21]. Following trypsinisation and centrifugation to extract the cells, the pellet was homogenized in 0.1 M potassium phosphate buffer (pH 7.4). An equivalent volume of 4% sulfosalicylic acid was added to 0.5 mL of this homogenate and then the mixture was allowed to precipitate the protein for an hour at 4 ºC. After centrifugation of the mixture, 0.03 mL of the supernatant was transferred into a new tube, where 0.066 mL of 5,5′-Dithiobis-(2-Nitrobenzoic Acid) (DTNB) reagent and 0.9 mL of 0.1 M potassium phosphate buffer were added. The quantity of reduced glutathione was calculated and represented as mM after the final reaction mixture was measured spectrophotometrically at 412 nm.

2.11 Lipid Peroxidation (LPO) Assay

The TBARS method, which was a slightly modified version of the previously described process, was used to

quantify the lipid peroxidation [22]. Cells were treated with NPs produced from *S. china*, and control cells were properly mixed in a cold KCl buffer. Then, 100 µL of the homogenate was mixed with 0.2 mL of 8.1% SDS, 1.5 mL of 20% acetic acid, 1.5 mL of 0.8% TBA reagent and 0.7 mL of sterile distilled water to generate a reaction mixture. To enable the synthesis of pink color, the mixture was heated for 60 min in a boiling water bath. Lipid peroxidation was expressed in µM, and the absorbance of the resultant solution was measured at 532 nm.

2.12 Cell Cycle - Flow Cytometry Analysis

The phase distribution and cellular DNA concentration were evaluated by fluorescence activated cell sorting (FACS) [23]. In summary, 1×10^6 cells were seeded on the flask, and then they were treated with 25, 50 and of CuO–ZnO produced from *S. china*. Following incubation, the cells were trypsinized and collected. To maintain a consistent single-cell suspension, the pellets were then fixed with 70% cold ethanol for the whole night at 4 ºC. RNase (0.1 mg/mL) was introduced to ensure selective DNA detection by removing RNA. After that, the cells were stained for 30 min at room temperature in the dark with 0.4 mL of propidium iodide (PI) solution (0.5 mg/mL). A BD FACS Calibur flow cytometer (Becton Dickinson, San Jose, CA, USA) was used to obtain fluorescence from PI-labeled nuclei, and the Cell Quest Pro software (3.2.1) (BD Biosciences, San Jose, CA, USA) was used to evaluate the results. An initial gate was established on the forward scatter (FSC) versus side scatter (SSC) plot to exclude cellular debris. Doublets and cell aggregates were excluded using PI fluorescence pulse-area versus pulse-width parameters (FL2-A versus FL2-W), and the resulting single-cell population was used for DNA content analysis.

2.13 Quantitative Analysis of Caspase Activity

The quantitative evaluation of caspase activity was carried out in accordance with the guidelines included in the commercial colorimetric test Kit (Elab science E-CK-A389, Wuhan, China). *S. china*–CuO–ZnO NPs at concentrations of 25, 50, and 75 µg/mL were added to the cells. Following this, the cells were collected, lysed in the provided buffer and then centrifuged. The Bradford technique was used to estimate the total protein levels in the supernatant. 200 µg of extracted protein was incubated with the chromogenic substrate, which releases peptide nucleic acid (pNA) upon enzymatic cleavage, in order to measure caspase-9 activity. Using a microtiter reader, the resulting color intensity was measured at 405 nm.

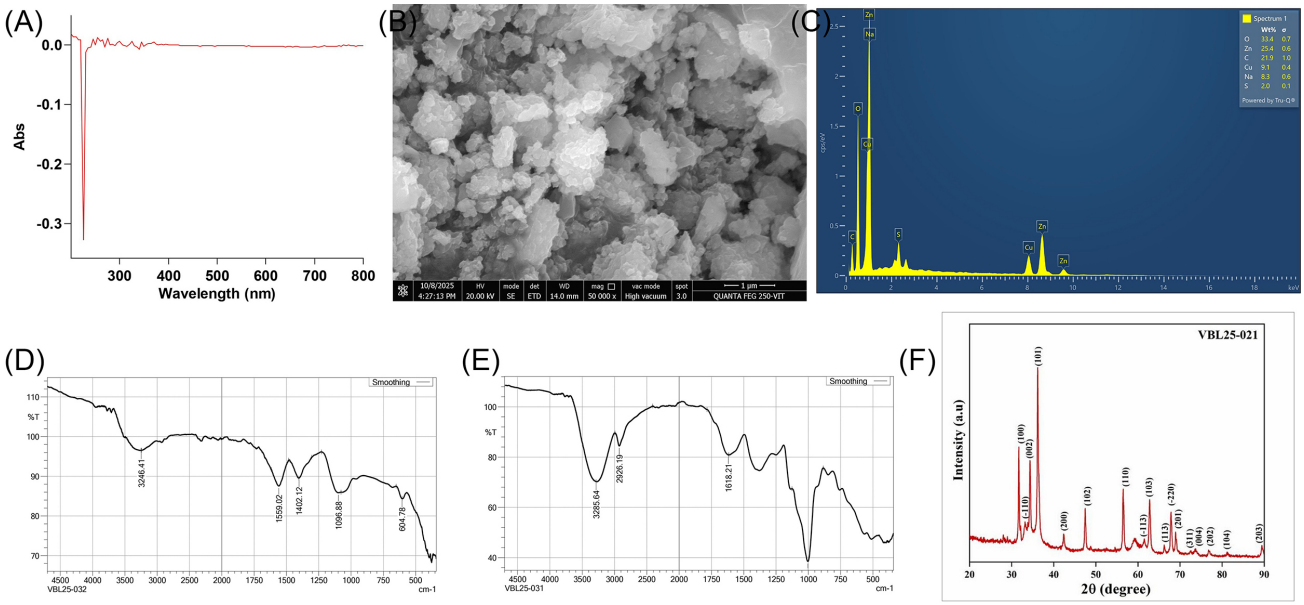


Fig. 1. Physicochemical characterization of biosynthesized CuO–ZnO bimetallic nanoparticles. (A) UV-visible absorption spectrum of the synthesized nanoparticles confirming nanoparticle formation. (B) Scanning electron microscopy (SEM) image showing the surface morphology and agglomerated nanoscale structure of the particles. (C) Energy dispersive X-ray (EDX) spectrum confirming the elemental composition of the nanoparticles, indicating the presence of Cu, Zn, and O, along with minor signals from biomolecules involved in stabilization. (D) FTIR spectrum of the *Smilax china* extracts showing characteristic functional groups responsible for the reduction and stabilization of metal ions. (E) FTIR spectrum of the synthesized CuO–ZnO nanoparticles demonstrating the involvement of phytochemical functional groups in nanoparticle formation and capping. (F) X-ray diffraction (XRD) pattern of the synthesized nanoparticles confirming their crystalline nature and the formation of CuO–ZnO bimetallic nanostructures. UV, Ultraviolet; FTIR, Fourier transform infrared spectroscopy.

2.14 Wound Healing Scratch Assay

Saos-2 cells were seeded at a density of 3×10^5 cells per well into 24-well plates and they were allowed to form a uniform growth over 24 h. A straight line "wound" was then created in each well using a sterile 20–200 µL pipette tip positioned vertically. The plates were gently agitated for 5 min at 500 rpm, and the dislodged cells were removed by washing with 500 µL of PBS. Fresh culture medium containing the desired concentrations of *S. china*-CuO–ZnO nanoparticles was subsequently added, and the cells were incubated for 24 h prior to image acquisition. Wells were washed with pre-warmed PBS and gently shaken for 30 sec. Fresh medium was then replenished and the wound area was monitored microscopically. Scratch closure was documented at 0, 12 and 24 h using an inverted microscope at 4× magnification [24].

2.15 Statistical Analysis

The test data's were carried out in triplicate, and the results were displayed as Mean ± SD. The statistical relationship between the treated and untreated groups was examined using GraphPad PRISM version 5.1 (Boston, MA, USA). Tukey's multiple comparison tests were used to compare the groups after a one-way ANOVA was completed. $p < 0.0001$ is regarded as statistically significant.

3. Results and Discussion

3.1 Synthesis and UV Characterization of S. china Mediated CuO–ZnO NPs

The synthesis of CuO–ZnO NPs was confirmed by the UV-visible spectra. Fig. 1A displays a distinctive absorption band in the UV region at 255 and 275 nm. The absence of a noticeable surface Plasmon resonance peak in the visible spectrum indicates that the phytochemical extracts effectively stabilized the nanoparticles and distributed them uniformly. The effective production of optically stable CuO–ZnO NPs is supported by a stable absorbance profile at higher wavelengths, indicating aggregation. Notably, the absence of a characteristic surface Plasmon resonance (SPR) band in the visible regions suggests good phytochemical stability as well as uniform particle dispersion. Green production of silver nanoparticles has been shown to have similar optical properties [9,10]. Particle clustering is responsible for the widened SPR bands. This is probably because the *S. china* extract has a high polyphenolic concentration.

3.2 SEM With EDAX Analysis

A study using SEM showed that the fabricated CuO–ZnO Nanoparticles have a noticeable agglomeration and an uneven quasi-spherical shape and hexagonal shape (Fig. 1B). The clustered formations are closely packed nano-sized grains as a result of capping mediated by phytochemicals during the synthesis process. The particle's nanoscale nature is further supported by the surface roughness and aggregation that have been observed. The comparatively regulated morphology indicates effective surface passivation, even though aggregation is commonly seen in green-synthesized NPs because of inter-particle hydrogen bonding and van der Waals interactions [25].

Fig. 1C shows that the elemental composition of the produced CuO–ZnO NPs was validated by EDAX analysis. Cu and Zn corresponding signals confirm the successful formation of bimetallic NPs. Minor peaks of Na and S most likely originate from plant residues, whereas the presence of C and O has been attributed to phytochemical capping from *Smilax china*. The high purity of the nanoparticles produced is indicated by the absence of unnecessary components. The presence of elemental CuO–ZnO, free of unnecessary impurity peaks, was confirmed by EDAX spectra, indicating successful bimetallic synthesis with good elemental purity. According to Mittal et al. (2013) [26], phytochemical-coated NPs are consistent with C and O signals, which are represented by organic capping molecules.

3.3 Fourier Transform Infrared Spectroscopy (FTIR)

The functional groups responsible for the reduction and stabilization of CuO–ZnO bimetallic NPs, Fourier transform infrared spectroscopy were performed. The *Smilax china* extracts FTIR spectrum (Fig. 1D) showed a large absorption band at 3246.41 cm^{-1}, which is indicative of the O-H stretching vibration of alcohols and phenolic compounds. C=C stretching of aromatic rings is responsible for the band seen at 1559.02 cm^{-1}, whereas C-H bending vibrations are linked to the peak at 1402.12 cm^{-1}. The presence of metal oxygen interaction is suggested by the low-frequency band at 604.78 cm^{-1}, while the absorbance band at 1096.88 cm^{-1} shows C-O stretching of polyphenols.

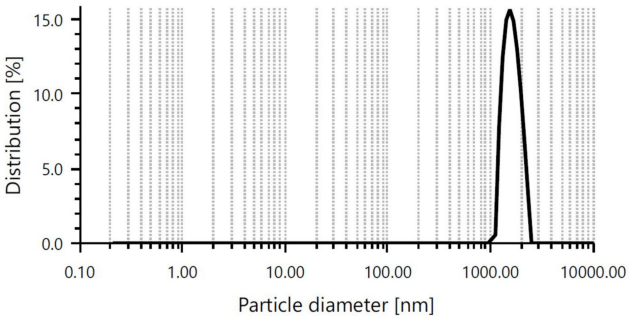


Fig. 2. Particle size distribution of CuO–ZnO NPs mediated by *S. china*. NPs, Nanoparticles.

The FTIR spectra of the synthesized CuO–ZnO bimetallic NPs (Fig. 1E) revealed a strong peak at 3285.64 cm^{-1}, indicating that phytochemicals effectively capped the molecules. The aliphatic C-H stretching vibrations are represented by the peak at 2926.19 cm^{-1}. The absorbance band at 1618.21 cm^{-1} may be ascribed to aromatic C=C vibration, suggesting that proteins or polyphenolic compounds are in-

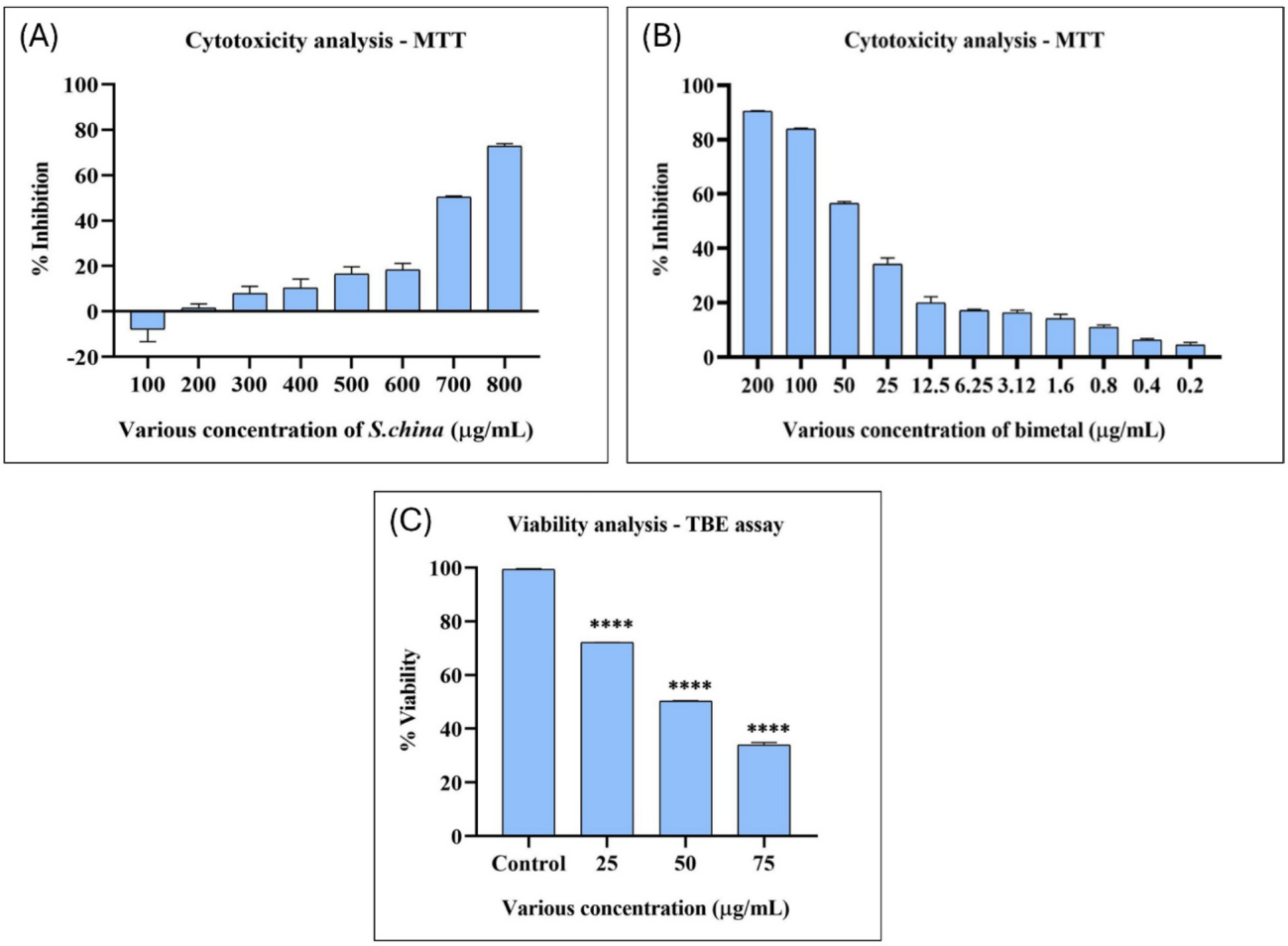


Fig. 3. Evaluation of cytotoxic effects and cell viability. (A) MTT cytotoxicity experiment displaying percentage inhibition at various concentrations of *S. china* extract and (B) CuO–ZnO NPs. (C) TBE assay for cell viability at various concentrations. MTT, 3-(4,5-dimethylthiazol-2-yl)-2,5-diphenyltetrazolium bromide; TBE, trypan blue exclusion. ****, $p < 0.0001$.

volved in the stability of nanoparticles. The involvement of bioactive ingredients in the reduction of metal ions and the fabrication of stable CuO–ZnO NPs is confirmed by the notable shift and decrease in intensity of the principal functional group peaks relative to the plant extract. According to FTIR analysis, the involvement of hydroxyl-rich phenolic and flavonoids in metal ion reduction and stabilization is confirmed by absorption peaks attributed to a wide O-H stretching band (~3246–3285 cm^{-1}), aromatic C=C vibration (~1559–1618 cm^{-1}), and C-O stretching band (~1096 cm^{-1}). Crucially, the observed peaks shifted after the synthesis of NPs, showing that biomolecules and metal surfaces have strong coordination interactions. O-H, C=O, and C-O vibration bands were attributed to phytoconstituent reduction and capping interactions during NPs formation. Similar FTIR transition involving hydroxyl-rich phenolic and other phytochemical functional groups have been reported in green-synthesized CuO–ZnO NPs from *Eryngium foetidum* leaf extract and *Rubia cordifolia* L [14,27].

3.4 XRD Analysis

The X-ray diffraction (XRD) pattern of *Smilax china*-mediated CuO–ZnO bimetallic nanoparticles indicates successful synthesis, with diffraction peaks at 2θ values of approximately 31.8°, 34.4°, 36.3°, 47.5°, 56.6°, 62.9°, 66.4°, 67.9°, 69.1°, 72.6°, 76.9°, 81.3°, and 89.6°, corresponding to various crystallographic planes (Fig. 1F). These peaks confirm the crystallinity of the nanoparticles, aligning with the hexagonal wurtzite structure for ZnO (JCPDS No. 36-1451) and the monoclinic structure for CuO (JCPDS No. 48-1548). The sharp peaks suggest high crystallinity and phase purity, confirming the incorporation of both metal oxides within the bimetallic structure. Similar findings have been noted in earlier studies linking enhanced crystallinity to the stabilizing effects of plant-derived phytochemicals during synthesis [28].

3.5 Particle Size Analyzer (PSA)

According to PSA studies, the produced CuO–ZnO bimetallic nanoparticles (Fig. 2) had a narrow and independent particle size distribution around 1000 nm, indicat-

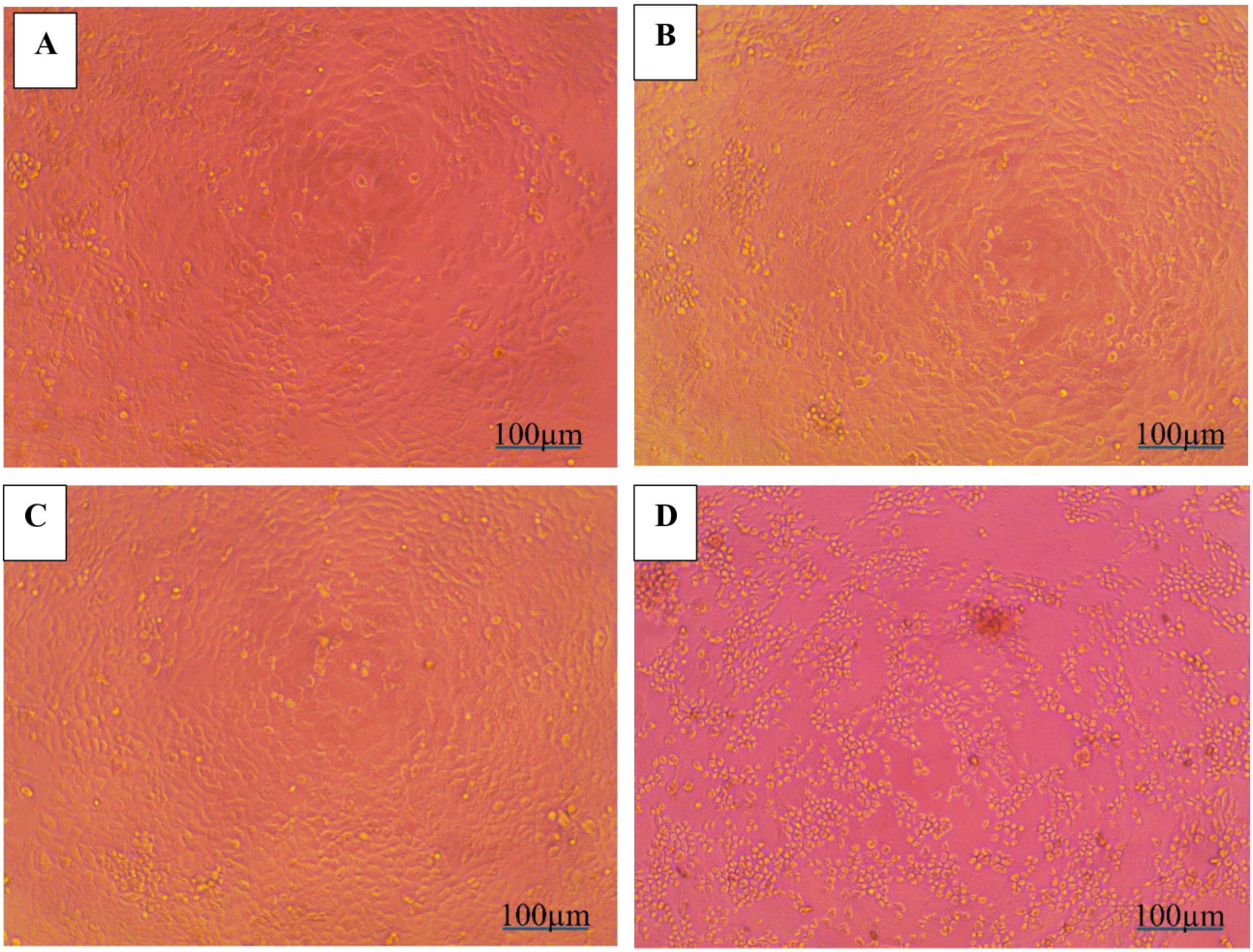


Fig. 4. Morphometric evaluation of *S. china*–CuO–ZnO NPs exposed to the Saos-2 cell line. Control, 25 µg/mL, 50 µg/mL, and 75 µg/mL concentrations are represented by (A), (B), (C), and (D), respectively. (Scale bar = 100 µm).

ing a monomial and relatively uniform distribution with low polydispersity. The particle size observed by SEM was in the nanometer range, representing the primary size of the dried nanoparticles. In contrast, the particle size obtained from the PSA was larger, which can be attributed to the aggregation of nanoparticles in suspension. Such differences between microscopic and suspension-based particle size measurements are commonly reported because suspended nanoparticles tend to form agglomerates due to interparticle interactions. Usually, the phytochemical capping agents are responsible for this stability. Ahmed et al. (2016) [10] reported that plant phytochemicals act as reducing agents in the synthesis of metal oxide nanoparticles. Such successful surface passivation could improve cellular uptake and cell interactions.

3.6 MTT Analysis of S. china Plant Extract and Synthesized CuO–ZnO NPs

The cytotoxicity assay was used to assess the MTT effects of the bimetallic formulation and S. China extract at different concentrations. Over the range of 100–800 µg/mL, *S. china* extract demonstrated a concentration-dependent increase in cytotoxicity as seen in Fig. 3A. A pronounced cytotoxic effect was evident at higher concentrations, with 50.57% inhibition at 700 µg/mL and nearly 73.03% inhibition at 800 µg/mL concentration. In contrast, at relatively low doses, bimetallic NPs showed significant cytotoxic activity (Fig. 3B). 25–50 µg/mL concentration of NPs showed 50% cytotoxicity compared to control ($p < 0.0001$). The bimetal nanoparticles (CuO–ZnO) were more potent than the *S. china,* but both treatments showed dose-dependent cytotoxic effect. According to earlier research [14], CuO–ZnO NPs have more anti-cancer activity than monometallic nanoparticles, attributed to higher redox cycling and ROS production. The MTT results were supported by the trypan blue exclusion assay, which showed concentration-dependent decrease in cell viability.

3.7 TBE Analysis

Synthesized CuO–ZnO NPs doses of 25, 50, and 75 µg/mL were selected based on the MTT analysis. Untreated control cells had 100% viability, as shown in Fig. 3C. Cell

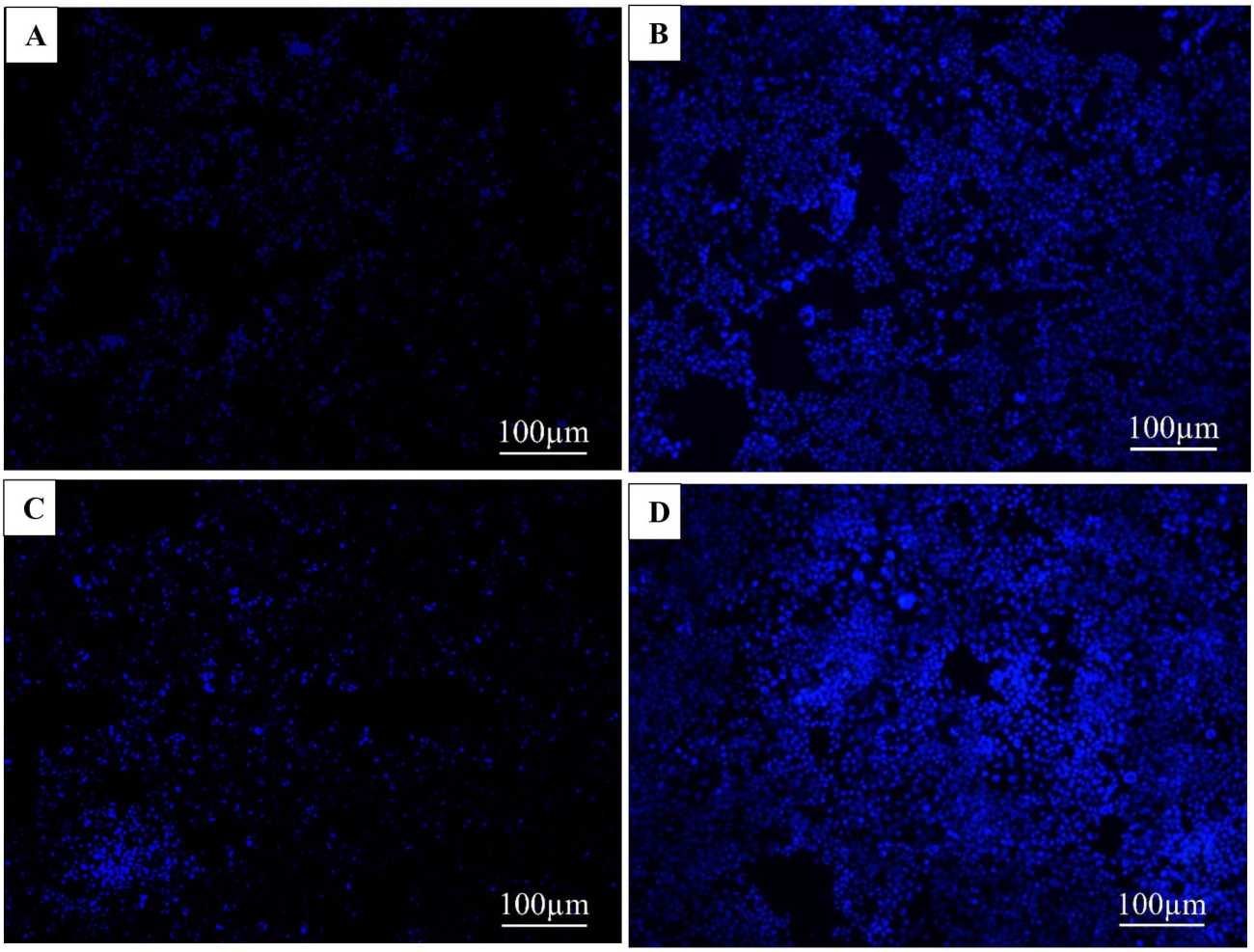


Fig. 5. DAPI staining: Fluorescence microscopic images showing nuclear morphological changes in *S. china* –CuO–ZnO NPs treated Saos-2 cells. (A: Control, B: 25 µg/mL, C: 50 µg/mL and D: 75 µg/mL). DAPI, 4′,6-diamidino-2-phenylindole. (Scale bar = 100 µm).

viability was significantly reduced to about 70% after treatment with 25 µg/mL; at 50 µg/mL, cell viability was reduced to 50%, and 30–35% viability was observed at 75 µg/mL relative to the control (****, $p < 0.0001$). Overall, the findings show that cell viability decreases with an increase in NPs concentration.

3.8 Morphological Analysis

Using phase-contrast microscopy, concentration-dependent mortality rates were evaluated by morphological analysis of Saos-2 cells treated with NPs (Fig. 4A–D). Normal spindle-shaped morphology, intact adhesion, and uniform distribution were shown in control cells (Fig. 4A). In 25 µg/mL, lower morphological changes were observed (Fig. 4B), whereas a higher dose of 75 µg/mL showed cell rounding, cell shrinkage, and loss of adhesion (Fig. 4D). Sathishkumar et al. (2009) [25] reported Similar morphological changes.

3.9 Fluorescence Analysis by DAPI Staining

Fluorescence microscopy revealed that the nuclear staining intensity in Saos-2 cell lines was concentration-dependent following treatment (Fig. 5A–D). Normal cell intensity and intact nuclear morphology were indicated by the control cells (Fig. 5A). The fluorescence intensity of cells treated with 25 µg/mL (Fig. 5B) increased noticeably, indicating the early signs of cytotoxicity. The fluorescent signal increased and nuclear distribution changed at 50 µg/mL (Fig. 5C) with cell damage. Extensive cell death was consistent with the strong fluorescence and noticeable nuclear condensation observed following treatment with 75 µg/mL (Fig. 5D). These observations strengthen the cytotoxicity and cell viability assay results by confirming a dose-dependent cytotoxic response in Saos-2 cells. Increased nuclear damage and cell shrinkage were evidenced by a gradual increase in fluorescence intensity with rising nanoparticle concentrations [29]

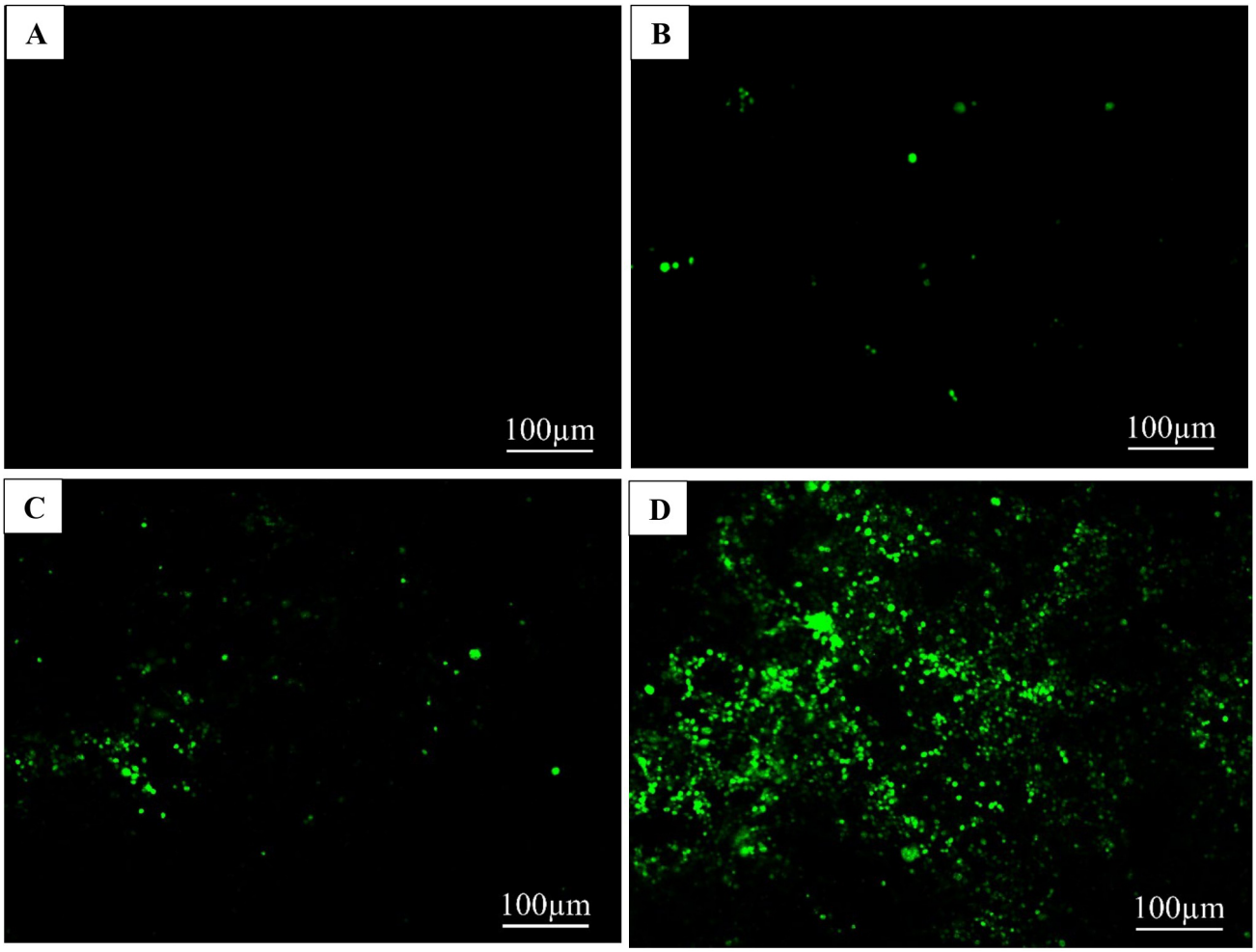


Fig. 6. Intracellular reactive oxygen species (ROS) generation detected by using DCFH-DA staining. (A: Control, B: 25 µg/mL, C: 50 µg/mL and D: 75 µg/mL). DCFH-DA, 2′,7′-dichlorodihydrofluorescein Diacetate. (Scale bar = 100 µm).

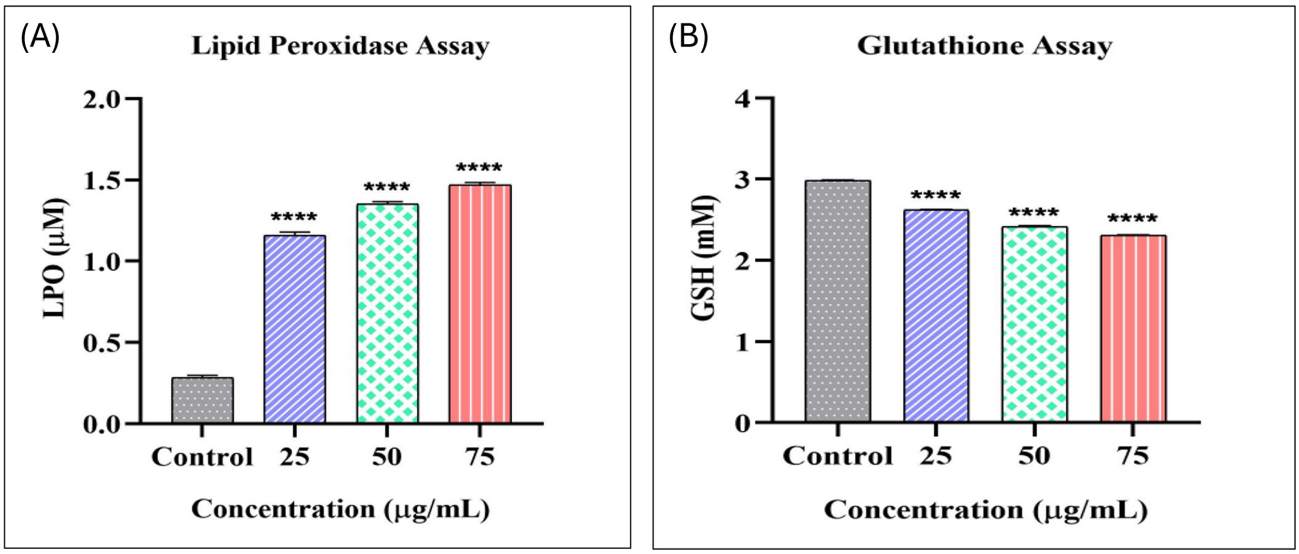


Fig. 7. Estimation of lipid peroxidation and glutathione by enzymatic assays. The LPO assay (A) showed a gradual increase in a concentration-dependent manner, while the GSH assay (B) demonstrated a notable decrease dependent on concentration. All the results were statistically analyzed. LPO, lipid peroxidation; GSH, glutathione. ****, $p < 0.0001$.

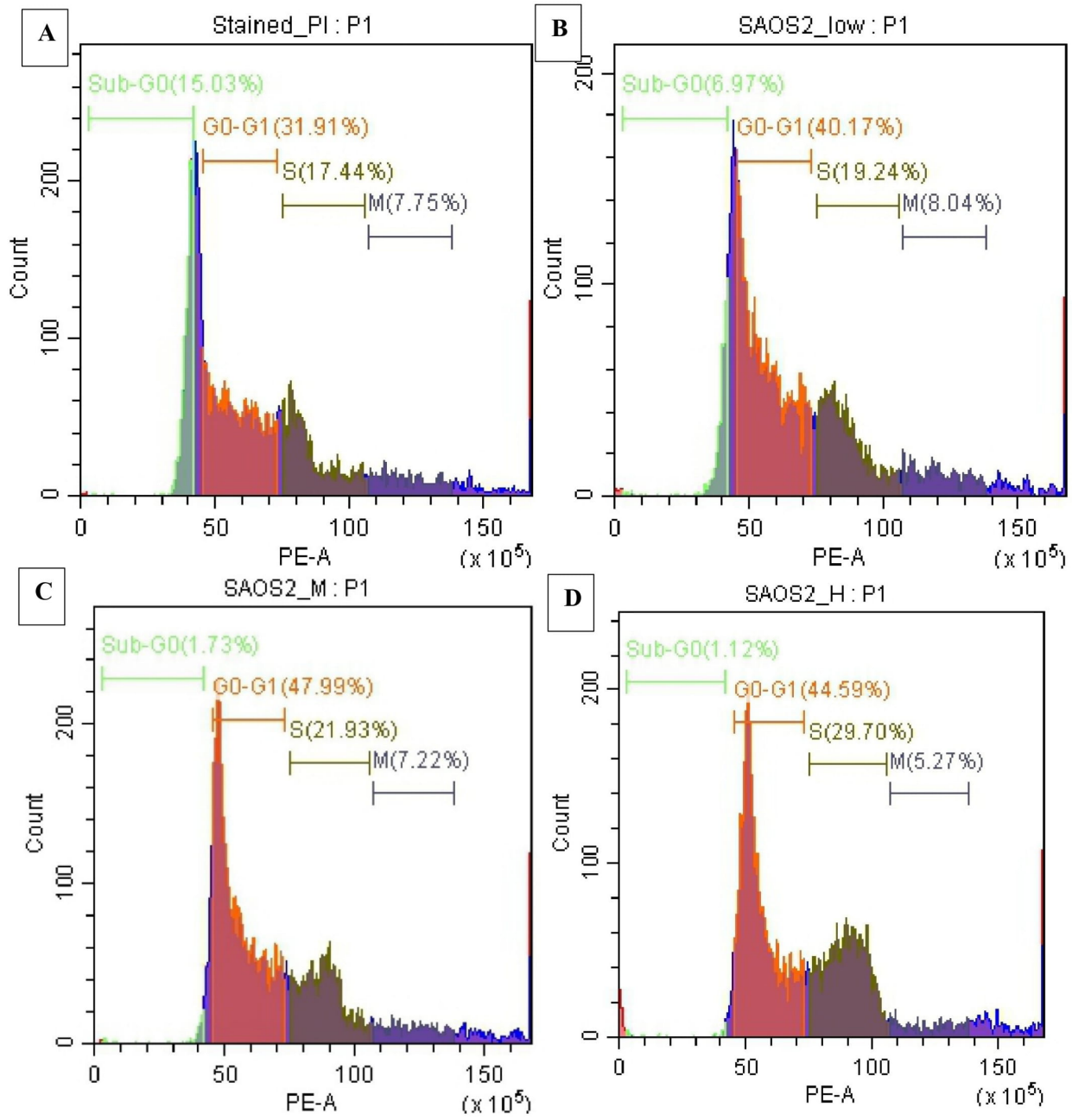


Fig. 8. Cell cycle analysis of Saos-2 cells by flow cytometry. (A), (B), (C) and (D) stand for Control, 25 µg/mL, 50 µg/mL and 75 µg/mL concentrations.

3.10 Evaluation of Oxidative Stress Markers (ROS, LPO and GSH)

A fluorescence-based ROS assay was used to measure the amount of intracellular ROS produced in Saos-2 cells (Fig. 6A–D). Green fluorescence was low in control cells (Fig. 6A), indicating low ROS levels. The fluorescence intensity of cells treated with 25 µg/mL (Fig. 6B) increased slightly, indicating early ROS generation. The increased green fluorescence at 50 µg/mL (Fig. 6C) indicated a significant increase in ROS production. Excessive ROS generation was indicated by the bright and broad fluorescence that followed treatment with 75 µg/mL (Fig. 6D).

LPO levels in Saos-2 cells were markedly elevated following treatment with *S. china*–CuO–ZnO NPs compared with the control group. LPO levels increased significantly after exposure to 25, 50, and 75 µg/mL concentrations, respectively (Fig. 7A). In contrast, intracellular GSH levels decreased significantly in a concentration-dependent manner. At 25, 50, and 75 µg/mL, GSH levels decreased to 2.62 ± 0.06, 2.41 ± 0.05, and 2.29 ± 0.04 mM, respectively (Fig. 7B). A significant increase in treatment groups relative to control was confirmed using Turkey's multiple comparison analysis (****$p < 0.0001$).

Intracellular ROS levels increased in a concentration-dependent manner, as indicated by DCFH-DA staining. Increased production of ROS can cause oxidative damage to proteins, lipids, and DNA, which causes mitochondrial death [14]. This mechanism was supported by a considerable increase in LPO and a depletion of intracellular GSH. Oxidative stress involvement is confirmed by decreased antioxidant levels and increased LPO, which are frequently observed in nanoparticles that induce cytotoxicity [7].

3.11 Cell Cycle Analysis

Cell cycle analysis was performed to investigate the effect of *Smilax china*-mediated CuO–ZnO bimetallic nanoparticles on cell cycle progression in Saos-2 osteosarcoma cells (Fig. 8). Untreated control cells (A) exhibited 31.91% of cells in the G0/G1 phase, 17.44% in the S phase, and 7.75% in the G2/M phase, with a Sub-G0 population of 15.03%. Following treatment with 25 µg/mL nanoparticles (B), the G0/G1 population increased to 40.17%, while the S and G2/M populations were 19.24% and 8.04%, respectively, with the Sub-G0 fraction decreasing to 6.97%. Treatment with 50 µg/mL nanoparticles (C) further increased the G0/G1 population to 47.99%, accompanied by 21.93% cells in the S phase and 7.22% in the G2/M phase, whereas the Sub-G0 population was 1.73%. At the highest concentration (75 µg/mL, D), the G0/G1 population remained elevated (44.59%), while the S phase markedly increased to 29.70% and the G2/M phase was 5.27%, with only 1.12% of cells in the Sub-G0 phase. These findings indicate that CuO–ZnO nanoparticles altered normal cell cycle progression, resulting in G0/G1 and S phase accumulation in Saos-2 cells. Similarly, cell cycle arrest was observed in Glioma cells treated with synthesized Au-CuO and CuO–ZnO nanoparticles [15].

3.12 Caspase-9 Activity

The activity of caspase 9 in Saos-2 cells was measured after treatment with different concentrations of NPs (25, 50, and 75 µg/mL) (Fig. 9). Basal caspase activity was seen in control cells. Compared with the control, the 25 µg/mL treatment showed a small increase in caspase-9 release. On the other hand, caspase-9 activity was significantly elevated at 50 µg/mL ($p < 0.05$) and then increased at 75 µg/mL (*$p < 0.01$). These findings support the intrinsic apoptotic pathways in treated Saos-2 cells by showing concentration-dependent activation of caspase-9. One possible component of cell death is the activation of pro-apoptotic pathways, which begin with the release of cytochrome c and mitochondrial membrane permeabilization [30,31,32]. The current study examined *S. china* mediated CuO–ZnO NPs affected the activation of Caspase-9 in Saos-2 cancer cells. There was increased caspase activity, which is consistent with apoptosis induction.

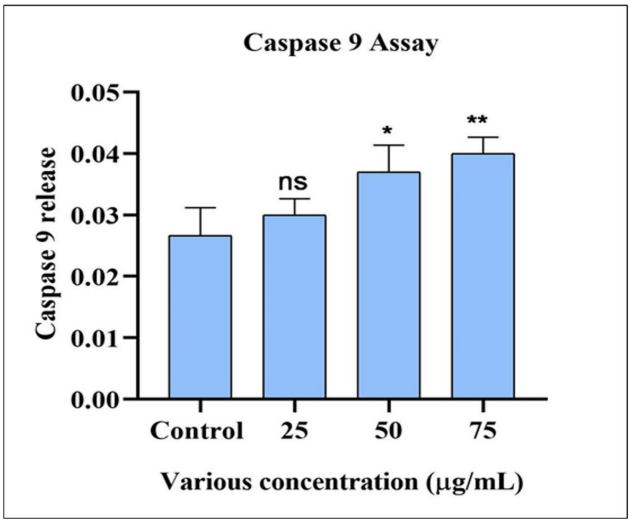


Fig. 9. Caspase 9 activities in Saos-2 cells. Cells treated with *S. china*–CuO–ZnO bimetallic NPs at 25 µg/mL, 50 µg/mL and 75 µg/mL. A significant elevation was observed at higher concentrations. Statistical analysis was performed using one-way ANOVA followed by Tukey's multiple comparison tests. ns, Not significant ($p > 0.05$); *$p < 0.05$; **$p < 0.01$ compared with the control.

3.13 Wound Healing Assay

A wound healing assay was used to assess the impact of NPs on the migration of Saos-2 cells (Fig. 10). Rapid migration of the control cells caused significant wound closure during the incubation period. On the other hand, a larger wound area and delayed closure in comparison to the control indicated that the treated cells exhibited a concentration-dependent inhibition of cell migration. Cell migration into the scratched area significantly decreased with an increase in NPs concentrations. This confirms the anti-metastatic activity. The reduced migratory capacity may be attributed to cytoskeletal alterations and ROS-mediated disruption of intracellular signaling pathways. Similar suppression of cancer cell migration has been reported for CuO–ZnO nanocomposites, highlighting their therapeutic relevance beyond cytotoxicity [14].

Collectively, these findings indicate that *Smilax china*-mediated CuO–ZnO nanoparticles exert enhanced anticancer effects through a multifaceted mechanism involving oxidative stress amplification, antioxidant depletion, lipid peroxidation, mitochondrial apoptosis (caspase-9 activation), cell cycle arrest, and inhibition of cell migration. These results support the potential application of green-synthesized CuO–ZnO nanoparticles as promising therapeutic candidates for osteosarcoma.

3.14 Limitations

This study has several limitations that should be considered when interpreting the findings. First, the anticancer activity of *Smilax china*-mediated CuO–ZnO nanoparticles was evaluated using only the Saos-2 osteosarcoma cell line;

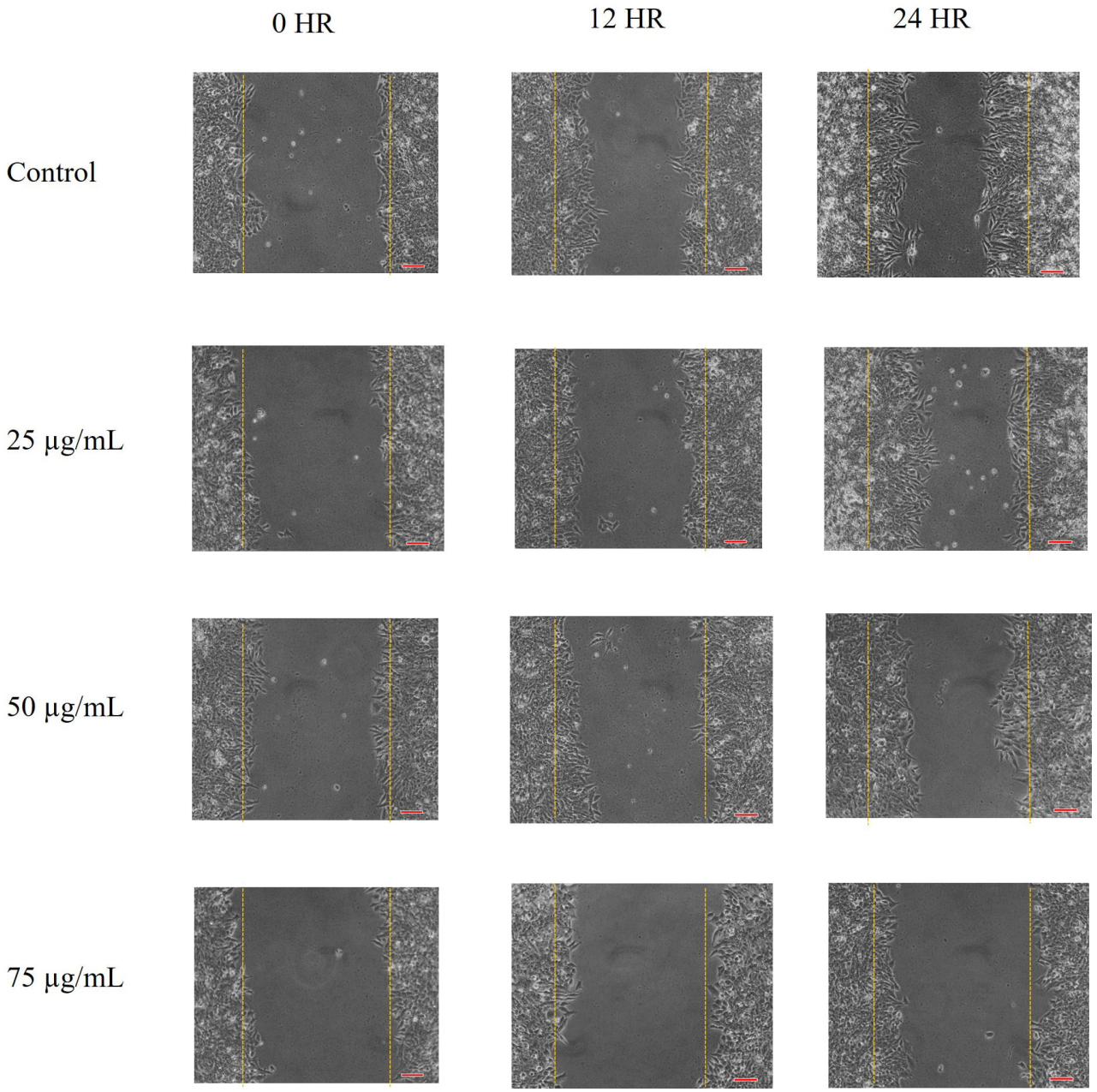


Fig. 10. Effect of *S. china* CuO–ZnO NPs on Saos-2 cells by wound healing assay at 0 h, 12 h and 24 h. Reduced wound closure in treated groups indicates inhibition of cell migration. (Scale bar = 100 µm).

therefore, the findings may not fully represent the biological heterogeneity of osteosarcoma. Evaluation in additional osteosarcoma cell lines and non-malignant osteoblastic cells would be valuable to establish the selectivity and broader anticancer potential of the nanoparticles. Second, although increased ROS generation, lipid peroxidation, GSH depletion, cell-cycle alterations, and caspase-9 activation support the involvement of oxidative stress and apoptosis, the molecular pathways responsible for these effects were not investigated in detail. In addition, the contribution of ROS to nanoparticle-induced cytotoxicity was not confirmed using antioxidant or ROS-scavenging experiments. Finally, the present study was limited to *in vitro* experiments, and the pharmacokinetics, biodistribution, systemic toxicity, and antitumor efficacy of the nanoparticles remain to be established in appropriate *in vivo* models. Further mechanistic and preclinical studies are therefore required before their potential therapeutic application in osteosarcoma can be established.

4. Conclusion

This study successfully demonstrated the green synthesis of *Smilax china*-mediated CuO–ZnO bimetallic nanoparticles with high crystallinity, phase purity, and good colloidal stability. The synthesized nanoparticles exhibited significantly enhanced cytotoxic activity against Saos-

2 cells compared to the plant extract alone. Mechanistic investigations revealed that the anti-cancer activity was primarily mediated through excessive ROS generation, depletion of intracellular GSH, increased lipid peroxidation, cell cycle arrest at the G0/G1 and S phases and activation of caspase-9–dependent intrinsic apoptosis. Additionally, the nanoparticles effectively inhibited cancer cell migration, indicating potential anti-metastatic properties. The synergistic interaction between the Cu and Zn components appears to amplify oxidative stress and apoptotic signaling, thereby enhancing therapeutic efficacy. Overall, these findings highlight the potential of eco-friendly synthesized CuO–ZnO nanoparticles as viable candidates for osteosarcoma therapy and warrant further *in vivo* validation and translational investigations.

Abbreviations

ATCC, American Type Culture Collection; DAPI, 4′,6-Diamidino-2-phenylindole; DCFH-DA, 2′,7′-Dichlorodihydrofluorescein diacetate; DMEM, Dulbecco's Modified Eagle Medium; DMSO, Dimethyl Sulfoxide; DNA, Deoxyribonucleic Acid; DTNB, 5,5′-Dithiobis-(2-Nitrobenzoic Acid); EDAX, Energy Dispersive Analysis of X-rays; EDX, Energy Dispersive X-ray Spectroscopy; FACS, Fluorescence Activated Cell Sorting; FBS, Fetal Bovine Serum; FTIR, Fourier Transform Infrared Spectroscopy; GSH, Reduced Glutathione; LPO, Lipid Peroxidation; MDR, Multidrug Resistance; OS, Osteosarcoma; PSA, Particle Size Analyzer; ROS, Reactive Oxygen Species; SEM, Scanning Electron Microscopy; SPR, Surface Plasmon Resonance; XRD, X-ray Diffraction.

Availability of Data and Materials

The data supporting the findings of this study are available from the corresponding author upon reasonable request.

Author Contributions

AHM: conceptualization, methodology, investigation, data curation, formal analysis, and writing—original draft preparation. EMS: supervision, project administration, conceptualization, validation, writing—review and editing, and correspondence. KMS: methodology, software, formal analysis, visualization, data interpretation and writing—review and editing. KIZ: investigation, resources, data collection, validation, and writing—review and editing. ZMA: statistical analysis, interpretation of results, visualization, and writing—review and editing. All authors read and approved the final version of the manuscript. All authors have participated sufficiently in the work and agreed to be accountable for all aspects of the work.

Ethics Approval and Consent to Participate

Not applicable.

Acknowledgment

Not applicable.

Funding

Ongoing Research Funding program, (ORF-2026-1970), King Saud University, Riyadh, Saudi Arabia.

Conflicts of Interest

The authors declare no conflicts of interest.

References

[1] Kansara M, Teng MW, Smyth MJ, Thomas DM. Translational biology of osteosarcoma. Nature Reviews. Cancer. 2014; 14: 722–735. https://doi.org/10.1038/nrc3838

[2] Isakoff MS, Bielack SS, Meltzer P, Gorlick R. Osteosarcoma: Current Treatment and a Collaborative Pathway to Success. Journal of Clinical Oncology: Official Journal of the American Society of Clinical Oncology. 2015; 33: 3029–3035. https://doi.org/10.1200/JCO.2014.59.4895

[3] Pelicano H, Carney D, Huang P. ROS stress in cancer cells and therapeutic implications. Drug Resistance Updates: Reviews and Commentaries in Antimicrobial and Anticancer Chemotherapy. 2004; 7: 97–110. https://doi.org/10.1016/j.drup.2004.01.004

[4] Ferrando R, Jellinek J, Johnston RL. Nanoalloys: from theory to applications of alloy clusters and nanoparticles. Chemical Reviews. 2008; 108: 845–910. https://doi.org/10.1021/cr040090g

[5] Tardito S, Marchiò L. Copper compounds in anticancer strategies. Current Medicinal Chemistry. 2009; 16: 1325–1348. https://doi.org/10.2174/092986709787846532

[6] Prasad AS. Zinc: an antioxidant and anti-inflammatory agent: role of zinc in degenerative disorders of aging. Journal of Trace Elements in Medicine and Biology: Organ of the Society for Minerals and Trace Elements (GMS). 2014; 28: 364–371. https://doi.org/10.1016/j.jtemb.2014.07.019

[7] Manke A, Wang L, Rojanasakul Y. Mechanisms of Nanoparticle-Induced Oxidative Stress and Toxicity. BioMed Research International. 2013; 1: 942916. https://doi.org/10.1155/2013/942916

[8] Almoneef MM, Awad MA, Aldosari HH, Hendi AA, Aldehish HA, Merghani NM, et al. Enhancing Biomedical and Photocatalytic Properties: Synthesis, Characterization, and Evaluation of Copper–Zinc Oxide Nanoparticles via Co-Precipitation Approach. Catalysts. 2024; 14: 641. https://doi.org/10.3390/catal14090641

[9] Iravani S. Green synthesis of metal nanoparticles using plants. Green Chemistry. 2011; 13: 2638–2650. https://doi.org/10.1039/c1gc15386b

[10] Ahmed S, Ahmad M, Swami BL, Ikram S. A review on plants extract mediated synthesis of silver nanoparticles for antimicrobial applications: A green expertise. Journal of Advanced Research. 2016; 7: 17–28. https://doi.org/10.1016/j.jare.2015.02.007

[11] Wu ST, Zhao Y, Piao XL, Qiu L, Huang Y, Cheng XG. The active components of Smilax china L. against cancer by interfering with the interactions among associated proteins. Journal of Functional Foods. 2023; 106. https://doi.org/10.1016/j.jff.2023.105591

[12] Lee SE, Ju EM, Kim JH. Free radical scavenging and antioxidant enzyme fortifying activities of extracts from Smilax china root. Experimental & Molecular Medicine. 2001; 33: 263–268. https://doi.org/10.1038/emm.2001.43

[13] Rodan SB, Imai Y, Thiede MA, Wesolowski G, Thompson D,

Bar-Shavit Z, et al. Characterization of a human osteosarcoma cell line (Saos-2) with osteoblastic properties. Cancer Research. 1987; 47: 4961–4966.

[14] Daimari J, Deka AK. Anticancer, antimicrobial and antioxidant activity of CuO-ZnO bimetallic nanoparticles: green synthesised from Eryngium foetidum leaf extract. Scientific Reports. 2024; 14: 19506. https://doi.org/10.1038/s41598-024-69847-w

[15] Dobrucka R, Kaczmarek M, Łagiedo M, Kielan A, Długaszewska J. Evaluation of biologically synthesized Au-CuO and CuO-ZnO nanoparticles against glioma cells and microorganisms. Saudi Pharmaceutical Journal: SPJ: the Official Publication of the Saudi Pharmaceutical Society. 2019; 27: 373–383. https://doi.org/10.1016/j.jsps.2018.12.006

[16] Mosmann T. Rapid colorimetric assay for cellular growth and survival: application to proliferation and cytotoxicity assays. Journal of Immunological Methods. 1983; 65: 55–63. https://doi.org/10.1016/0022-1759(83)90303-4

[17] Crowley LC, Marfell BJ, Christensen ME, Waterhouse NJ. Measuring Cell Death by Trypan Blue Uptake and Light Microscopy. Cold Spring Harbor Protocols. 2016; 2016: 10.1101/pdb.prot087155. https://doi.org/10.1101/pdb.prot087155

[18] Moongkarndi P, Kosem N, Kaslungka S, Luanratana O, Pongpan N, Neungton N. Antiproliferation, antioxidation and induction of apoptosis by Garcinia mangostana (mangosteen) on SKBR3 human breast cancer cell line. Journal of Ethnopharmacology. 2004; 90: 161–166. https://doi.org/10.1016/j.jep.2003.09.048

[19] Raja Singh P, Arunkumar R, Sivakamasundari V, Sharmila G, Elumalai P, Suganthapriya E, et al. Anti-proliferative and apoptosis inducing effect of nimbolide by altering molecules involved in apoptosis and IGF signalling via PI3K/Akt in prostate cancer (PC-3) cell line. Cell Biochemistry and Function. 2014; 32: 217–228. https://doi.org/10.1002/cbf.2993

[20] Farooqui A, Khan F, Khan I, Ansari IA. Glycyrrhizin induces reactive oxygen species-dependent apoptosis and cell cycle arrest at G_0/G_1 in $HPV18^+$ human cervical cancer HeLa cell line. Biomedicine & Pharmacotherapy = Biomedecine & Pharmacotherapie. 2018; 97: 752–764. https://doi.org/10.1016/j.biopha.2017.10.147

[21] Goh BH, Kadir AH. In vitro cytotoxic potential of Swietenia macrophylla King seeds against human carcinoma cell lines. Journal of Medicinal Plants Research. 2011; 5: 1395–1404.

[22] Ohkawa H, Ohishi N, Yagi K. Assay for lipid peroxides in animal tissues by thiobarbituric acid reaction. Analytical Biochemistry. 1979; 95: 351–358. https://doi.org/10.1016/0003-2697(79)90738-3

[23] Siddiqui S, Arshad M. Osteogenic potential of punica granatum through matrix mineralization, cell cycle progression and runx2 gene expression in primary rat osteoblasts. Daru: Journal of Faculty of Pharmacy, Tehran University of Medical Sciences. 2014; 22: 72. https://doi.org/10.1186/s40199-014-0072-7

[24] Wang X, Decker CC, Zechner L, Krstin S, Wink M. In vitro wound healing of tumor cells: inhibition of cell migration by selected cytotoxic alkaloids. BMC Pharmacology & Toxicology. 2019; 20: 4. https://doi.org/10.1186/s40360-018-0284-4

[25] Sathishkumar M, Sneha K, Won SW, Cho CW, Kim S, Yun YS. Cinnamon zeylanicum bark extract and powder mediated green synthesis of nano-crystalline silver particles and its bactericidal activity. Colloids and Surfaces. B, Biointerfaces. 2009; 73: 332–338. https://doi.org/10.1016/j.colsurfb.2009.06.005

[26] Mittal AK, Chisti Y, Banerjee UC. Synthesis of metallic nanoparticles using plant extracts. Biotechnology Advances. 2013; 31: 346–356. https://doi.org/10.1016/j.biotechadv.2013.01.003

[27] Prasad A, Sidhic J, Mohan CS, Sarbadhikary P, George S, Narayanankutty A, et al. Biogenic synthesis of metal oxide nanoparticles for the elicitation of secondary metabolites in the in vitro propagated plantlets of Rubia cordifolia L. Plant Cell, Tissue and Organ Culture. 2025; 160: 66. https://doi.org/10.1007/s11240-025-03009-2

[28] Endeshaw SB, Goddati M, Lee J, Aga FG, Tufa LT, Sabir FK. ZnO/CuO nanocomposites for enhanced photocatalytic and antibacterial applications: A comparative study of synthesis methods. Journal of Science: Advanced Materials and Devices. 2025; 10: 100898. https://doi.org/10.1016/j.jsamd.2025.100898

[29] Elmore S. Apoptosis: a review of programmed cell death. Toxicologic Pathology. 2007; 35: 495–516. https://doi.org/10.1080/01926230701320337

[30] Abdel-Daim MM, Eissa IAM, Abdeen A, Abdel-Latif HMR, Ismail M, Dawood MAO, et al. Lycopene and resveratrol ameliorate zinc oxide nanoparticles-induced oxidative stress in Nile tilapia, Oreochromis niloticus. Environmental Toxicology and Pharmacology. 2019; 69: 44–50. https://doi.org/10.1016/j.etap.2019.03.016

[31] Singh S. Zinc oxide nanoparticles impacts: cytotoxicity, genotoxicity, developmental toxicity, and neurotoxicity. Toxicology Mechanisms and Methods. 2019; 29: 300–311. https://doi.org/10.1080/15376516.2018.1553221

[32] Li Y, Li F, Zhang L, Zhang C, Peng H, Lan F, et al. Zinc oxide nanoparticles induce mitochondrial biogenesis impairment and cardiac dysfunction in human iPSC-derived cardiomyocytes. International Journal of Nanomedicine. 2020; 2669–2683. https://doi.org/10.2147/IJN.S249912